Temperature Advection by Tropical Instability Waves

MARKUS JOCHUM AND RAGHU MURTUGUDDE

National Center for Atmospheric Research, Boulder, Colorado

(Manuscript received 7 March 2005, in final form 26 August 2005)

ABSTRACT

A numerical model of the tropical Pacific Ocean is used to investigate the processes that cause the horizontal temperature advection of tropical instability waves (TIWs). It is found that their temperature advection cannot be explained by the processes on which the mixing length paradigm is based. Horizontal mixing of temperature across the equatorial SST front does happen, but it is small relative to the "oscillatory" temperature advection of TIWs. The basic mechanism is that TIWs move water back and forth across a patch of large vertical entrainment. Outside this patch, the atmosphere heats the water and this heat is then transferred into the thermocline inside the patch. These patches of strong localized entrainment are due to equatorial Ekman divergence and due to thinning of the mixed layer in the TIW cyclones. The latter process is responsible for the zonal temperature advection, which is as large as the meridional temperature advection but has not yet been observed. Thus, in the previous observational literature the TIW contribution to the mixed layer heat budget may have been underestimated significantly.

1. Introduction

Tropical instability waves (TIWs) are a phenomenon common to both the Atlantic and the Pacific Oceans (Dueing et al. 1975; Legeckis 1977). Their surface structure can be seen best in satellite pictures of sea surface temperature (Chelton et al. 2000) and ocean color (Fig. 1) where they can be observed in the eastern part of the basins between 4°S and 4°N as cusplike features with wavelengths between 600 and 2000 km and phase speeds between 20 and 60 cm s^{-1}. However, optical sensors have to be used with care as they rely on the presence of surface property gradients to identify TIWs. Altimeters, too, are only of limited help since the high frequency and short wavelength of TIWs can lead to an aliasing of the observations (Musman 1986, 1992; Katz 1997). For example, the waves visible in Fig. 1 cannot be identified with Ocean Topography Experiment (TOPEX)/Poseidon (G. Goni 2003, personal communication). The subsurface structure and the frequency domain of TIWs have been studied with current meter moorings by Weisberg and Weingartner (1988), Qiao and Weisberg (1998), and Bryden and Brady (1989). The mooring records show in both oceans surface amplitudes of zonal and meridional velocity of up to 50 cm s^{-1} with a central periodicity of approximately 25 days. The energy reaches a maximum at the surface and the center of the basin along the equator and decays rapidly below 50 m. Still, signals of TIWs were found as deep as 800 m (Boebel et al. 1999).

Early analytical studies by Philander (1976, 1978) demonstrate that the equatorial zonal currents are barotropically unstable and preferentially generate waves with wavelengths and periods of the observed TIWs. A series of highly idealized numerical studies corroborated these findings but showed that baroclinic (Cox 1980), frontal (Yu et al. 1995), and Kelvin–Helmholtz instabilities (Proehl 1996) can contribute as well. Cox (1980) pointed out that what is simply referred to as TIWs is a superposition of unstable waves and their projection on the set of free equatorial waves. These idealized studies help to connect the complex observations of TIWs with the well-understood phenomena of equatorial waves and instabilities of zonal flows. However, Proehl (1996) pointed out that this approach ceases to be helpful in understanding the details of the wave–zonal flow interaction that characterizes the TIWs and equatorial currents. Most importantly, it fails to explain the preferred wavelength of TIWs. Proehl (1996) uses the overreflection theories of Lindzen (1988) to explain the wavelength and phase speed of TIWs as a function of spatial scale and amplitude of the zonal mean flow.

Corresponding author address: Markus Jochum, National Center for Atmospheric Research, P.O. Box 3000, Boulder, CO 80307.
E-mail: markus@ucar.edu

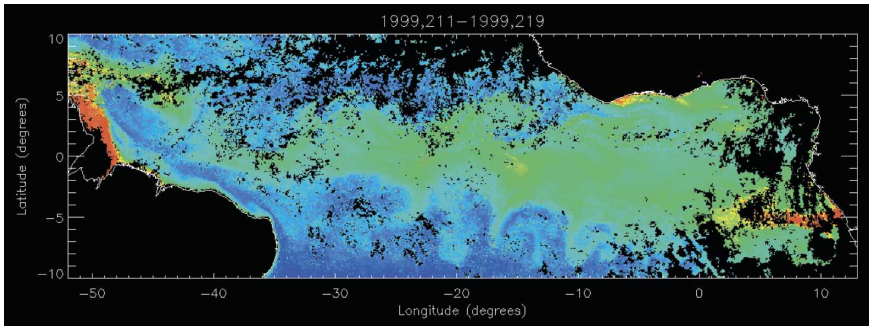

FIG. 1. TIWs as seen by Sea-Viewing Wide Field-of-View Sensor (SeaWiFS; from Jochum et al. 2004a). Note the cusps in ocean color along 4°S and 4°N.

Because of the wide basin and the strong zonal currents in the equatorial Pacific it is tempting to use the wave–mean flow interaction theories for TIWs. These theories (known as transformed Eulerian mean, or TEM) have been developed by Eliassen and Palm (1961), Boyd (1976), and Andrews and McIntyre (1976) for the atmospheric circulation. A key assumption in these theories is that the flow field can be averaged zonally. Because zonal averages are not suitable for oceanographic purposes, there have been efforts in formulating an eddy-forcing theory for time–mean flows analogous to TEM (Hoskins et al. 1983; Plumb 1986; Cronin 1996). The basic physics that underlies these theories (and TEM) is that eddies can accelerate or generate a mean flow directly through advection of momentum or indirectly through advection of layer thickness. The latter case causes a steepening of the isotherms, which accelerates the flow via the thermal wind relation. A direct comparison of these two effects is not straightforward, but for the *zonal mean* case, TEM provides a technique to combine both processes into the momentum equation. With the quasigeostrophic approximation, a similar technique can also be applied to the *time mean* fields in the ocean. It is key, however, that the eddy fluxes can be separated into a divergence-free and a rotation-free component. This separation is not unique and has to be argued for on a case-by-case basis (Plumb 1983; Marshall and Shutts 1981; Cronin 1996; Fox-Kemper et al. 2003). TEM-like approaches have been applied at and near the equator by Proehl (1990) and Jochum and Malanotte-Rizzoli (2004, 2005), each with different, limiting assumptions. While all the aforementioned studies provide important insights into eddy dynamics, the exact quantification of the eddy–mean flow interaction remains elusive. For the present study, we will assume the dynamics of the flow field as given and investigate how it affects the mixed layer heat budget.

A detailed understanding of how the TIWs affect the mixed layer is necessary because of their potential importance for climate. The aforementioned mooring data and drifter observations by Hansen and Paul (1984) and Baturin and Niiler (1997) suggest a meridional equatorward heat flux divergence of more than 100 W m^{-2}, and the strong effect of TIWs on equatorial plankton and nutrient distribution has been observed by Chavez et al. (1999) and Menkes et al. (2002). New insights into ocean–atmosphere coupling have been gained by analyzing the correlation between high-resolution wind fields and SST: the strong SST gradients induced by TIWs locally change the wind, which in turn leads to additional wind stress curls and divergences (Hashizume et al. 2001; Chelton et al. 2001).

Their short time and length scales and their global importance make it necessary to study TIWs with numerical models. Very recently numerical models became sophisticated enough to simulate TIWs accurately and already it has become apparent that TIWs can only be understood by the combined use of theory, models, and observations. For the Atlantic, TIWs have been shown to create the oxygen and salinity front in the intermediate waters along the equator (Jochum and Malanotte-Rizzoli 2003), drive the Tsuchiya jets (Jochum and Malanotte-Rizzoli 2004), and because of their chaotic nature contribute to the interannual variability of SST in the tropical Atlantic (Jochum et al. 2004b) and Pacific (Jochum and Murtugudde 2004).

Despite their importance for the tropical climate, not much has been learned about *how* TIWs affect SST. The ways in which mooring and drifter observations have been designed and analyzed suggest that it is assumed that the main effect of TIWs is that they move warm water meridionally toward the equator. Wave breaking (Kessler et al. 1998) then creates filamentation and isolated patches of temperature anomalies on which small-scale diffusion can act efficiently. Thus, warm water provided by the North Equatorial Countercurrent (NECC) and recently upwelled cold water

from the Equatorial Cold Tongue (ECT) are exchanged across the SST front along 2°N; the process is two-dimensional, restricted to the horizontal plane. However, close inspection of SST images (like Chelton et al. 2001) or ocean color (e.g., Fig. 1) does not show warm-core eddies as they are observed in the Gulf Stream. Also, the results of Jochum et al. (2004a) show that the meridional heat flux of TIWs can in part be compensated for by an associated vertical heat flux. This is because—at least in their model—the water below the mixed layer (ML) flows largely adiabatically along isotherms. In areas of steep isothermal slope, such as near the equator, measuring only the horizontal component can overestimate the total heat flux convergence. All of the aforementioned authors are very careful about the interpretation of data, but it is clear that the impact of TIWs on the equatorial heat budget is a three-dimensional problem that is not very well constrained by observations.

In a first attempt to understand the impact of TIWs on the equatorial ML heat budget, Jochum et al. (2005) compared the results of a coarse- and a high-resolution OGCM. They found that in the coarse-resolution OGCM the numerical horizontal diffusion moves temperature across the SST front at 2°N, consistent with the idea that wave breaking, which can be parameterized as diffusion, is responsible for the warming of the ECT. In the high-resolution OGCM, however, TIWs did not cool the warm waters north of the equator to heat the ECT. Instead, they increased the atmosphere–ocean heat flux near the equator. Thus, TIWs act as a vertical heat pump, rather than a horizontal mixer of temperature. The focus of Jochum et al. (2005) was the large-scale SST, not the detailed processes by which TIWs change the SST. Here, we will explain in detail how in a numerical model TIWs affect the ML heat budget.

The next section describes the numerical model. Since the observational database is larger in the Pacific Ocean, it is focused on numerical results from the Pacific. Identical experiments have been performed for the Atlantic Ocean and the results are qualitatively similar. The third section discusses the physical mechanisms responsible for the TIW temperature advection and a summary and discussion are provided in section 4.

2. Model description

The ocean model employed for this study is the reduced-gravity, primitive equation, sigma-coordinate model of Gent and Cane (1989). It is coupled to an advective atmospheric mixed-layer model that computes surface heat fluxes without any restoring boundary conditions or feedbacks to observations (Seager et al. 1995; Murtugudde et al. 1996). A variable-depth oceanic mixed layer represents the three main processes of oceanic turbulent mixing, namely, the entrainment–detrainment due to wind and buoyancy forcing, the gradient Richardson number mixing generated by the shear flow instability, and the convective mixing related to static instabilities in the water column (Chen et al. 1994). The model is initialized with Levitus (1994) temperature and salinity fields, driven by seasonal Hellerman and Rosenstein (1983) winds. In this study, as well as in many previous studies on the tropical Atlantic, the first author found Hellerman and Rosenstein (1983) winds to generate currents and eddies consistent with observations.

The model has a ¼° horizontal resolution and 16 layers in the vertical. Their depth and thickness changes with time and location, but to provide some idea about the vertical resolution, the time mean layer depths at 0°, 140°W are listed here: 32, 35, 39, 46, 54, 69, 84, 113, 142, 198, 253, 363, 529, 768, 1044, 1320 m. At the meridional boundaries (at 20°N, S), temperature and salinity are restored to Levitus (1994). The model is spun up for 20 yr and the presented results are taken from the subsequent 5 yr of simulation (Fig. 2); the full model fields were saved every 5 days. It is important to note that with the atmospheric boundary layer model as the upper boundary condition, the model computes its own heat flux and can therefore develop its own SST. The SST is not artificially damped back to climatology, nor will a positive ocean–atmosphere feedback amplify small perturbations.

Since this study focuses on TIWs, it is important that it properly resolves and reproduces the observed eddy field in the tropical Pacific. We found that ¼° horizontal resolution is sufficient to reproduce the observed TIWs [for a summary of the observations, see Qiao and Weisberg (1995)]. While wavelength and period of simulated TIWs are relatively insensitive to viscosity (Cox 1980), their strength is not. For the present study, we found the strength of TIWs to be consistent with velocity observations of the Tropical Atmosphere–Ocean (TAO) array. Figure 3 illustrates the strength of TIWs at one particular location, which can be compared with the observations of Qiao and Weisberg (1995): TIWs are weak in spring and reach their maximum strength of ± 60 cm s^{-1} in the late summer. Lyman et al. (2005, unpublished manuscript) describes two separate centers of TIW activity at 140°W: one in high-pass-filtered eddy kinetic energy (EKE) on the equator with a period of approximately 20 days and one in high-pass-filtered temperature variance at 5°N with a period of approximately 30 days; both periods are

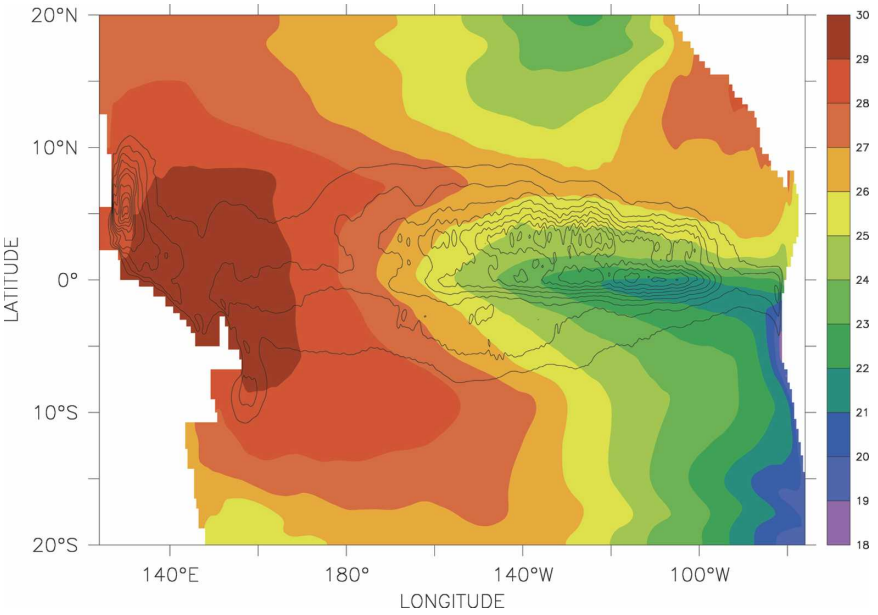

FIG. 2. Eddy kinetic energy with periods less than 60 days (contour line, 100 $cm^2\ s^{-2}$; maximum, 1100 $cm^2\ s^{-2}$) superimposed on the annual mean SST.

matched by the model (not shown). The full TAO time series from these locations show a surface maximum of EKE of 680 $cm^2\ s^{-2}$ and a subsurface maximum of temperature variance of 3.5°$C^2\ s^{-2}$ at 140-m depth. The respective model values are 620 $cm^2\ s^{-2}$ and 3.4°$C^2\ s^{-2}$ at 190-m depth. The magnitude of the SST variability caused by TIWs is also in accordance with observations; here and in the observations by Chelton et al. (2000), the SST difference between wave crest and trough is approximately 5°C.

3. Temperature advection of TIWs

The equations of the reduced-gravity, primitive-equation model in *s* coordinates are based on incompressible, hydrostatic equations of motion and the Boussinesq approximation. The equations for ML heat

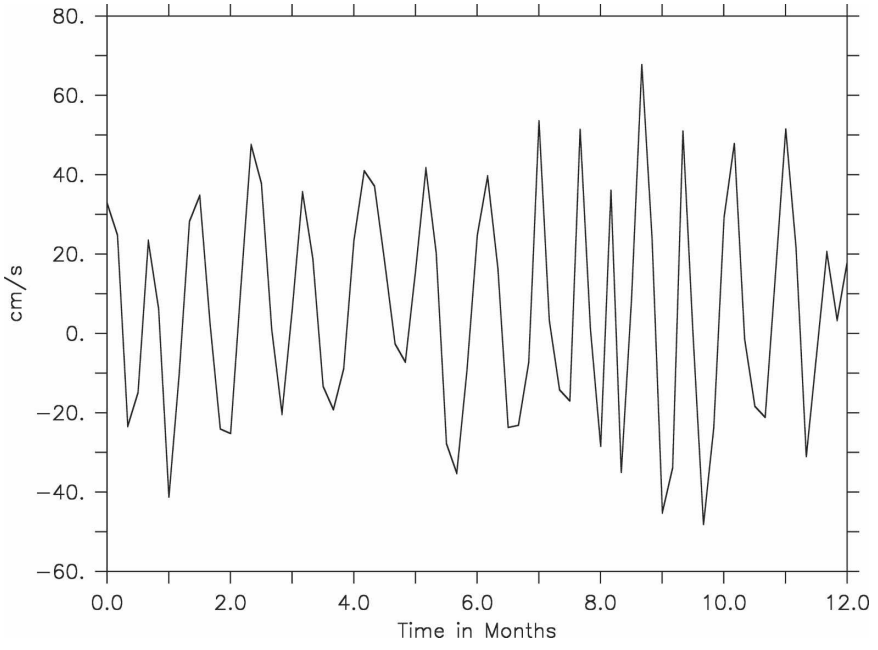

FIG. 3. Meridonal velocity in the mixed layer at the equator at 140°W.

and thickness that are discretized for the model are (Gent and Cane 1989)

$$\frac{\delta(hT)}{\delta t} + \nabla \cdot (\mathbf{u}hT) + \frac{\delta(w_e T)}{\delta s} = \frac{1}{\rho c_p}\frac{\delta Q}{\delta s} + hD \quad \text{and} \tag{1}$$

$$\frac{\delta h}{\delta t} + \nabla \cdot (\mathbf{u}h) + \frac{\delta w_e}{\delta s} = 0, \tag{2}$$

with $\mathbf{u}$ being the horizontal velocity vector, T temperature, h layer thickness, Q the net atmospheric heat flux, ρ the density of seawater, c_p its heat capacity, D the numerical diffusion operator (the Shapiro filter), and w_e the entrainment velocity computed by the Chen et al. (1994) ML model.

Heat content is a function of temperature and volume. Because of the incompressibility of seawater and our focus on irreversible processes (which excludes adiabatic waves), (1) and (2) are combined (Stevenson and Niiler 1983),

$$h\frac{\delta T}{\delta t} + h\mathbf{u} \cdot \nabla T + w_e \frac{\delta T}{\delta s} = \frac{1}{\rho c_p}\frac{\delta Q}{\delta s} + hD, \tag{3}$$

and dividing by the ML depth h yields (Kessler et al. 1998)

$$\frac{\delta T}{\delta t} + \mathbf{u} \cdot \nabla T + \frac{w_e}{h}\frac{\delta T}{\delta s} = \frac{1}{h\rho c_p}\frac{\delta Q}{\delta s} + D. \tag{4}$$

The division by h appears natural and significantly simplifies the following Reynolds averaging. There is, however, a potential ambiguity in the interpretation of the results. In the interior of the ocean much of the eddy effects on tracer distribution is thought to happen by Stokes drift or the bolus velocity (Gent and McWilliams 1990): the eddies advect the mean tracer gradient. It is typically expressed as $\overline{u'h'}/\overline{h}$ and dividing (3) by h causes the loss of information on the one part of eddy advection of which there is good theoretical understanding. However, in the case of TIWs the bolus velocity in the ML is less than 10% of the mean velocity. The only exception is the meridional component between 3° and 5°N, which can become as large as 20% of the mean flow and opposes the northward Ekman flow. These values are similar to the ones found by McWilliams and Danabasoglu (2002). Thus, the relative contribution of the terms in (3) is almost indistinguishable from those in (4) (not shown). Because of the division by h it is less important to observe ML depths (the definition of which is not unique anyway), and it simplifies the use of drifter and mooring data. In (4) the most troublesome observables, h and w_e, are combined in one single term that reduces the uncertainties in the temperature advection.

Reynolds averaging of (4) yields

$$\overline{\mathbf{u}_s \cdot \nabla T_s} + \overline{\mathbf{u}_s \cdot \nabla T'} + \overline{\mathbf{u}' \cdot \nabla T_s} + \overline{\mathbf{u}' \cdot \nabla T'} = \overline{q_{\text{atmos}}} - \overline{q_{\text{ent}}} + \overline{q_{\text{diff}}}, \tag{5}$$

where the overbar denotes the 5-yr mean; the SST and the velocities have been split into mean plus seasonal cycle (subscripts) and eddy component (superscript primes). The mean plus seasonal cycle has been determined by averaging over the monthly values of all years, the eddy components are the deviations from these mean plus seasonal values. The reason for this somewhat unusual split is that it facilitates the separation between seasonal waves and intraseasonal waves (TIWs). The first term on the lhs is the contribution of the mean and the seasonal cycle to the heat budget, the next three terms are the eddy contributions [since they would be zero without eddies; see Kessler et al. (1998)]. The correlation between the eddy terms and seasonal terms (terms 2 and 3 on the lhs) are negligible, which indicates a clean separation between seasonal waves and TIWs.

In principle it is also possible to separate the entrainment cooling $w_e\delta T$ in (4) into mean and eddy components, but we decided against it. The entrainment velocity is computed in the ML model based on buoyancy forcing and wind stirring. Furthermore, if the Richardson number is below 0.25, properties like temperature and momentum are vertically rearranged until the shear instability is removed. Layer thickness, however, is preserved and w_e is zero. In the next time step, buoyancy forcing or wind stirring can then efficiently mix a water column whose stratification has been weakened by shear instability (Chen et al. 1994). Thus, shear instability, buoyancy forcing, and wind stirring mutually affect each other, and because of this nonlinearity (especially near the equator) it is not possible to single out the contributions of the individual processes. This is discussed in detail in Schudlich and Price (1992).

Chen et al. (1994) estimated the empirical parameters of the mixed layer model from local synoptic data, but for the present context of TIWs, it is not clear whether these parameter values are still appropriate. However, the realistic representation of mean and seasonal SST in the current setting suggests that at least on these time scales the net entrainment cooling is reasonably well represented. On the correlation between w_e and δT on TIW and faster time scales, observations are simply not available, and rather than going through the significant computational expense of saving these terms at every single time step without having observational

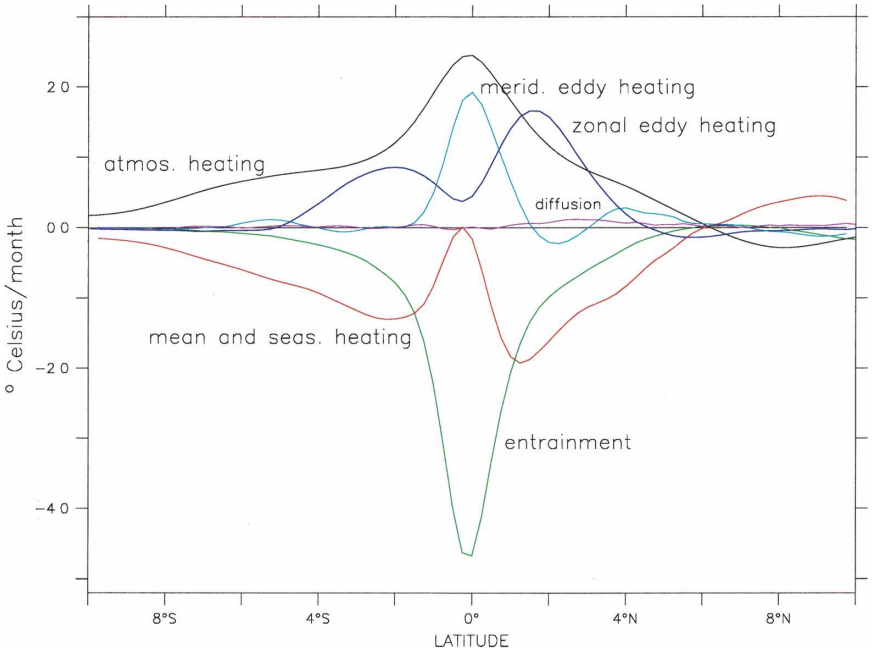

FIG. 4. Annual mean temperature budget for the tropical Pacific averaged between 145° and 135°W: black, net surface heat flux; red, mean and seasonal advection of temperature; dark blue, zonal eddy temperature advection; light blue, meridional eddy temperature advection; green, entrainment; and light purple, diffusion.

verification, we decided to save only 5-day averages of q_{ent}. The working hypothesis for the present study is that this q_{ent} is a reasonable representation of the diapycnal exchanges at the ML base. For the time scales of TIWs, there are no direct observations to prove this, but the discussion provides two independent and indirect sets of observations that suggest so. In addition, the focus of the present study is to reexamine the understanding on how TIWs affect SST rather than quantifying it.

The temperature budget (5) is shown in Fig. 4. The seasonal and mean advection of temperature is dominated by poleward Ekman divergence of freshly upwelled cold water. The atmospheric heat flux and the entrainment hold no surprises either: the entrainment is strongest at the equator because of the Ekman divergence there, and the resulting ECT induces a minimum of latent heat loss, which leads to a maximum in net atmospheric heat flux on the equator. The results are similar to the ones of Kessler et al. (1998), but here the foci are structure and value of the zonal and meridional eddy temperature advection. Several things make clear that traditional mixing length theory does not account for the temperature advection due to TIWs. First, if wave breaking would indeed be important, then temperature gradients would be moved to smaller scales and eventually be removed by horizontal diffusion. However, horizontal diffusion is almost negligible here (Fig. 4). Second, at length scales larger than those of TIWs, there is no significant zonal mean SST gradient that could explain the zonal temperature advection; and third, the equatorial heating that is due to temperature advection is not balanced by enough cooling anywhere. This is true even if we account for the latitudinally varying ML depth (Fig. 5). Averaged over the area from 4°S to 4°N and from the date line to 90°W, the zonal heat flux convergence contributes a net of 31 W m^{-2} and the meridional net contribution is 8 W m^{-2}. This is a significant portion of the average net atmospheric heat flux of 70 W m^{-2} over this domain. Thus, more than 50% of the equatorial atmosphere–ocean heat flux enters the ocean through and with the help of TIWs.

From the structure of the zonal and meridional temperature advection we conclude that TIWs do not mix temperature across the SST front; rather they increase the atmosphere–ocean heat flux and act as a vertical heat pump. Two things need explanation: how do TIWs redistribute temperature and how do they generate a net atmosphere–ocean heat flux? It turns out that the meridional and zonal temperature advections can be understood in a similar framework even though their spatial structures are rather dissimilar.

To understand the physics behind the meridional

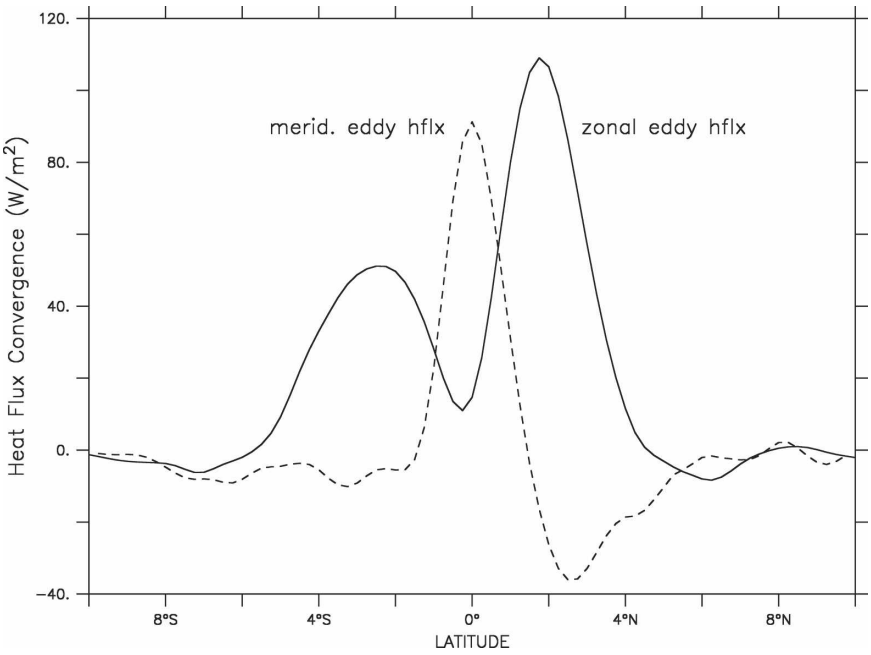

FIG. 5. Annual mean heat flux convergence averaged between 145° and 135°W: solid line, zonal eddy heat flux convergence; broken line, meridional eddy heat flux convergence.

temperature advection of TIWs, it is instructive to look at the temperature advection of the mean flow. The newly upwelled, cold ECT water is pushed poleward in the Ekman layer and heated by the atmosphere on its way to the subtropical gyres. In higher latitudes, it cools down again and mass is balanced by subduction and subsequent adiabatic geostrophic advection toward the equator (Pedlosky 1987; McCreary and Lu 1994). In extreme simplification, this can be thought of as flow in a closed pipe that, at the surface, is heated in the Tropics and cooled in midlatitudes. In the same pipe, one can also imagine temperature advection by an oscillatory flow. The water oscillates back and forth—every time it reaches the equator from the surface it is cooled because of strong vertical mixing and warmed when it flows poleward again (Fig. 6); the water parcels all retain their relative position but for the equator where they mix with those below. Thus, cooling is restricted to the equator. In the same pipe, heating and cooling could also be achieved by diffusion (the analog to wave breaking); then all water parcels would change their relative position and cooling would not be restricted to the equator. Since horizontal diffusion is negligible, the meridional temperature advection of the TIWs cannot be explained by wave breaking, but by the combination of their meridional oscillations with strong localized cooling on the equator: the meridional oscillation of the surface waters induced by the TIWs increases the area over which the ocean can absorb heat (this causes a net heat gain) and the vertical entrainment pumps this heat into the thermocline (Fig. 7). Thus, TIWs take heat that is accumulated in the off-equatorial ML and move it to the equator where it is removed by entrainment. This results in off equatorial cooling and equatorial warming (Fig. 5). A simple calculation can illustrate the power of this heat engine: the typical ML depth is 30 m, the average atmospheric heat flux is 100 W m^{-2} and the TIW wave period is about 30 days. In the absence of other processes, the water parcel would return to the ECT 1°C warmer, which yields the 2°C $month^{-1}$ heating rate of the TIWs (Fig. 4).

This distinction between oscillatory versus diffusive behavior is important for several reasons. First, parameterizing TIWs as diffusive in coarse-resolution OGCMs will lead to a lower off-equatorial SST (Jochum et al. 2005). Second, diffusion erodes the SST gradient whereas oscillation enhances it. The rapid cooling of the ML as the SST front approaches the equator acts almost like a boundary condition with a fixed (= thermocline) temperature. On the equatorward movement of the SST front, the distance between any isotherm and the equator shrinks, which increases the meridional SST gradient (Fig. 8). Extreme meridional SST gradients of 3°C over a distance of 10 km have indeed been observed across a TIW (Rudnick et al. 2002). As the water is pushed poleward again, the cross-frontal SST gradient relaxes because the latent heat loss is larger over the warmer SST. Thus, TIWs are neces-

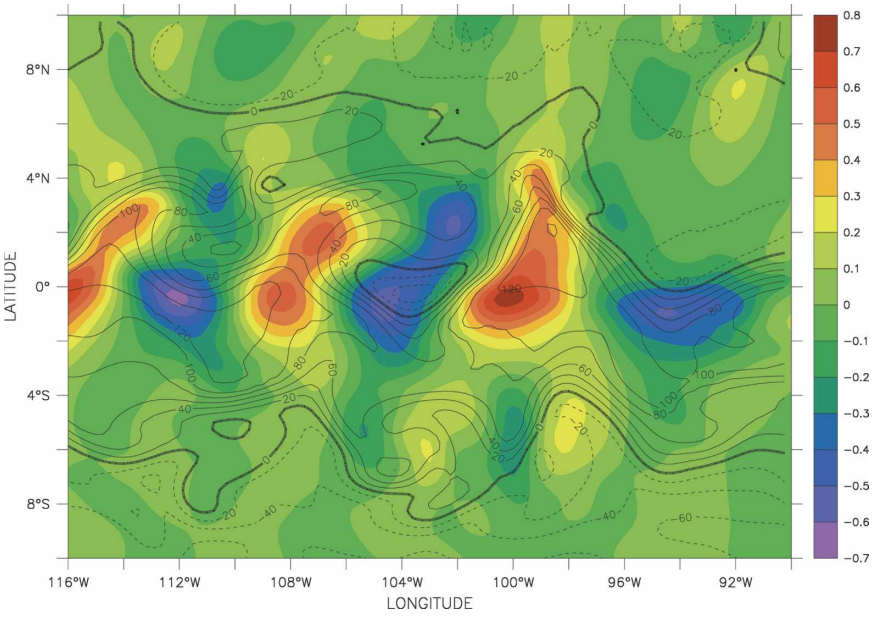

FIG. 6. Snapshot of ML meridional eddy velocity (m s^{-1}; color contours) and net atmospheric heat flux in June. It can be seen that the area of net ocean heat uptake is modulated by TIWs. Poleward flow is associated with larger heat uptake than equatorward flow because the water has been heated and the latent heat loss is increased. The superimposed flux contour lines have intervals of 20 W m^{-2}.

sary to explain the sharpness of the SST front north of the equator. In the absence of TIWs, the cold water that is pushed north in the Ekman layer would warm only gradually as it is heated by the atmosphere.

Like the meridional, the zonal temperature advection is made possible by the spatial inhomogeneities of the vertical mixing. In both cases energy for vertical mixing is provided by wind stirring and shear instability (in this model buoyancy forcing is negligible because of the absence of a diurnal cycle). However, meridional temperature advection relies on the equatorial singularity of the Ekman divergence, whereas TIWs by themselves create the spatial pattern of vertical mixing that is necessary to generate zonal temperature advection (Fig. 9). At the latitudes with large zonal temperature advection by TIWs, the mixed layer depth (MLD) perturbation caused by TIWs is well correlated with SST anomalies: a shallow ML causes a cold SST and vice versa (Fig. 10). When the ML is shallower, the same amount of mixing energy will reach into colder isotherms and bring colder water to the surface. This connection by itself is nothing new, it has been used to explain the positive feedbacks associated with El Niño (e.g., McCreary and Anderson 1984). However, to our knowledge this connection did not yet receive much attention in the study of TIWs. It becomes important in connection with its phase relation to the TIW's zonal velocity: warm water flows across isotherms toward cold water (Fig. 10). The only difference in the mechanism for meridional temperature advection is that the cold-water/large-mixing patch is not fixed in space but is an integral part of TIWs. This becomes clearer when one considers the analytical structure of equatorial free waves, which is derived, for example, in Philander (1990). Obviously, the TIWs are not free waves but their behavior and structure are similar nevertheless (Cox 1980; Masina and Philander 1999; Lyman et al. 2005). For the purpose of this argument TIWs can be thought of as projected onto Yanai and first latitudinal mode Rossby waves (Cox 1980). Both types of wave have off-equatorial maxima in the thermocline displacement (Philander 1990) but different phase relations between zonal velocity and thermocline displacements. Assuming that TIWs are free waves but SST anomalies are proportional to MLD anomalies, it is possible to compute the spatial structure of the expected zonal temperature advection from the analytical structure described in Philander (1990). For example, the zonal temperature advection for the first mode Rossby wave would be

$$uT_x = A \sin^2(kx - \omega t) e^{-\xi^2/2} \left(\frac{H_0}{\sigma + ck} + \frac{2^{1/2} H_2}{\sigma - ck} \right) \times \left(\frac{H_0}{\sigma + ck} - \frac{2^{1/2} H_2}{\sigma - ck} \right) M, \quad (6)$$

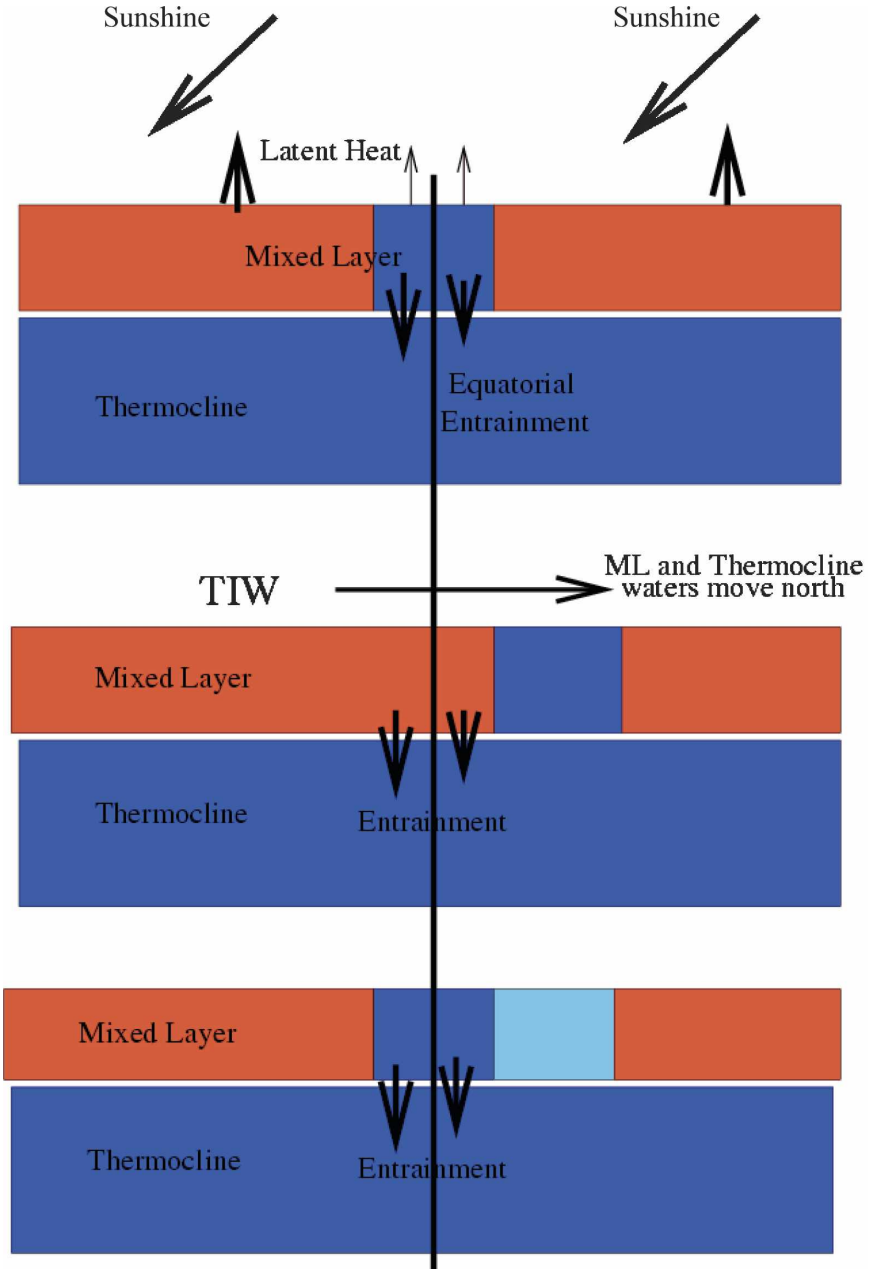

FIG. 7. Idealized representation of the mixing process described in the text. (top) A two-layer ocean at rest with localized vertical mixing at the equator. The mixed layer is uniformly warm, and the thermocline is uniformly deep and of infinite heat capacity. Ocean heat uptake is only possible near the equator; everywhere else the ML is in radiative balance with the atmosphere. (middle) In their first quarter period, the TIWs move the patch of ML cold water north and replace it with warm water. The old, cold water from the equator is now heated by the atmosphere, and the new warm water at the equator is cooled by vertical mixing. Since the cooling at the equator is larger than the heating poleward of it (Fig. 4), the area where the ocean can gain heat is larger than in the case without TIWs; therefore, (bottom) the TIWs cause a net heat gain. In the next quarter period, the new warm water is returned to the equator, and the above process is repeated south of the equator.

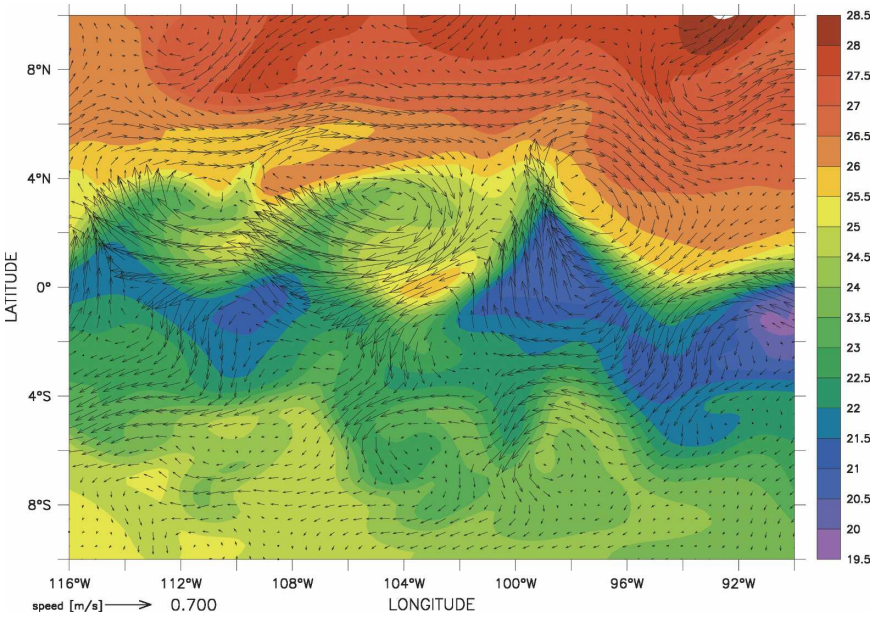

FIG. 8. Snapshot of SST and surface velocity in June. Note the strong meridional cross-isothermal flow on the equator at 94°W and the strong zonal cross-isothermal flow at 2°N, 106°W.

with k being the wavenumber for a wavelength of 700 km, σ the frequency for a period of 40 days, H_n the Hermite function of order n, c the equatorial Kelvin wave speed, and ξ the ratio between distance to the equator and equatorial Rossby radius. In addition, M reflects the connection between MLD and SST. This connection is dominant at the equator and is here set to be $M = e^{-\xi^4}$. For a TIW velocity scale of 20 cm s^{-1} and

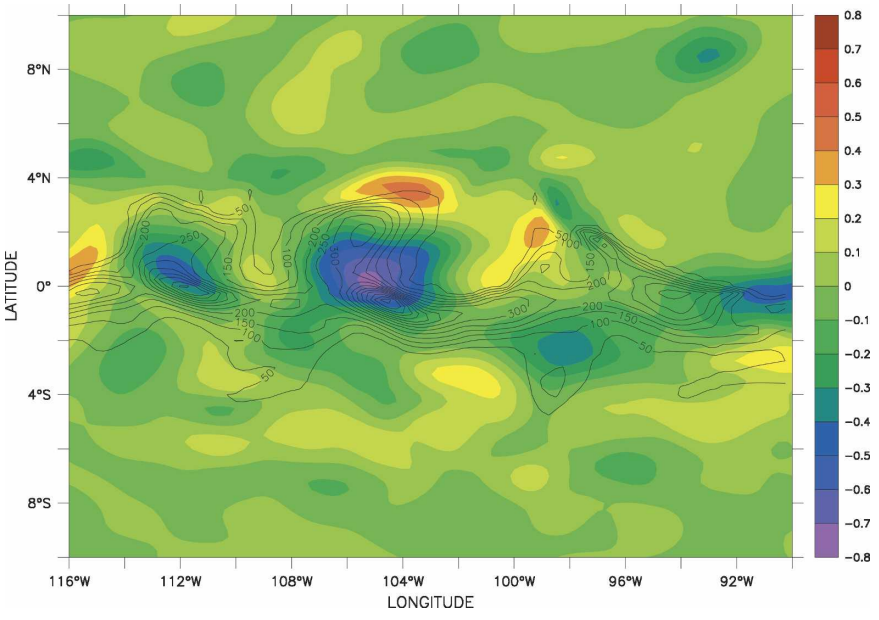

FIG. 9. Snapshot of ML zonal eddy velocity (m s^{-1}; color contours) and entrainment heat loss in June. It can be seen that the area of entrainment is modulated by TIWs. The poleward patches of large entrainment are associated with zonal eddy flow. The superimposed heat-loss contour lines have intervals of 50 W m^{-2}.

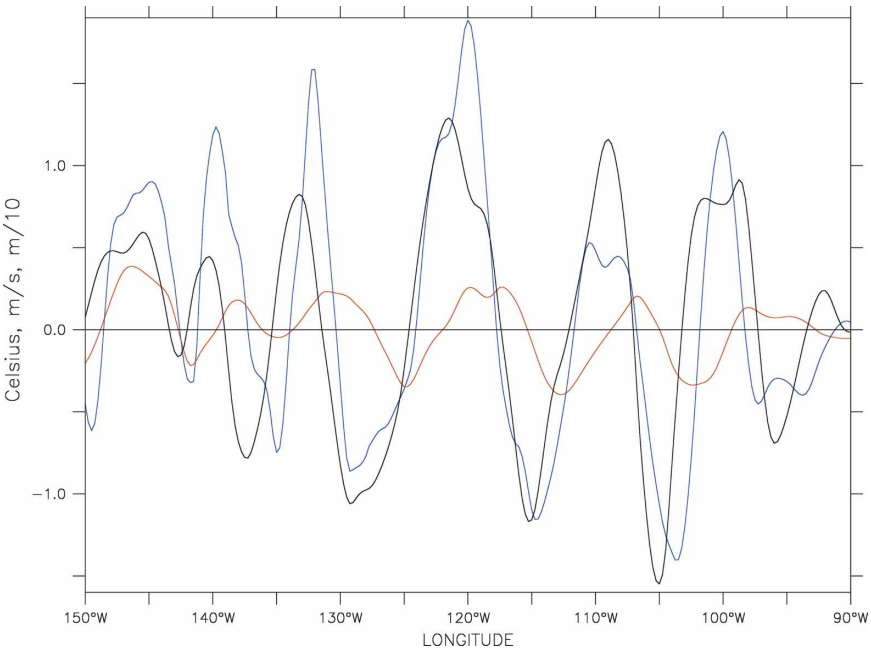

FIG. 10. Snapshot of high-pass-filtered SST (°C; black), MLD (m; blue), and zonal velocity (m s^{-1}; red) along 2°N during July. The correlation coefficients for 5 yr of high-pass-filtered model output from 150° to 100°W at 2°N are 0.62 between SST and MLD and 0.45 between the zonal velocity and MLD.

TIW-induced MLD anomalies of 10 m, the theoretical expression for the Rossby wave predicts the two maxima at 2°N and 2°S (cf. Fig. 4 with Fig. 11), and a temperature advection of approximately 1°C $month^{-1}$. Note that the different amplitude in TIW strength (Fig. 4) has been explained by Lyman et al. (2005) as the result of the mean zonal flow, which has not been taken into account here. A derivation for meridional tem-

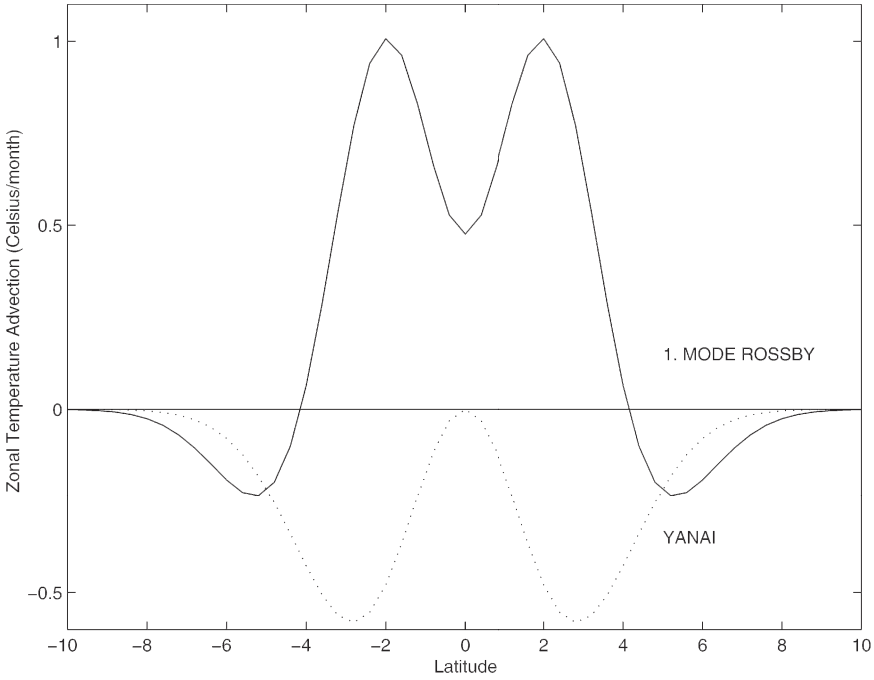

FIG. 11. Analytical expression for the expected zonal temperature advection of TIWs. See text for details.

perature advection, similar to the one for zonal temperature advection, leads to values of exactly zero because one essentially averages a sine function over one wavelength.

The analytical expression has also been derived for the Yanai wave and it predicts a cooling effect of the wave. Because of the asymmetry or irreversibility of the cooling–warming process, which has not been taken into account in the above expression, this is not a physical solution. A net temperature advection by the waves is possible because the flow is not geostrophically balanced close to the equator. The phase relation between u and MLD means that, in the case of the Rossby wave, warm water is pushed toward the shallower part of the ML. This causes a net entrainment of warm water. For the Yanai wave, however, cold water is pushed toward the deeper part of the ML. Because of the deep ML only limited mixing takes place, the process is reversible and no net temperature advection is produced.

It is not the purpose of the present study to find an exact analytical expression for temperature advection of TIWs; in the presence of friction, forcing, and large vertical diffusion this may not even be possible [for more details see Cox (1980) or McCreary (1981)]. Rather, the purpose is to highlight the possibility that TIWs make a significant net contribution to the equatorial ML heat budget by exploiting the shallowness of the ML there, and the irreversibility of vertical mixing.

The mechanisms for meridional and zonal temperature advection are similar but their spatial patterns are different. Both forms of temperature advection cause a net heating but only meridional temperature advection causes a substantial off-equatorial heat loss. This is because the entraining process is fixed in space and time for the meridional temperature advection only. Zonal temperature advection also cools locally to warm the patches of entrainment cooling. However, the vertical entrainment necessary for zonal temperature advection moves with the TIWs. By averaging in time and longitude, Figs. 4 and 5 reveal only the net effect, not the temporary and localized cooling as for meridional temperature advection.

4. Summary and discussion

Eddy temperature advection, the quantity evaluated here and observable in the ocean, is an abstract number that does not by itself reveal the underlying processes. Ideally, one would like to track individual particles in an experiment that isolates the process under investigation. Near the equator, however, this is close to impossible, even with a numerical model. The temperature budget (Fig. 4) as well as the momentum budget [for a detailed discussion see Pedlosky (1996)] show that the equator is a region that is controlled by a balance of always more than two processes. Moreover, thermodynamics strongly influences dynamics and vice versa (Schudlich and Price 1992); attributing cause and effect unequivocally is rarely possible. This is also the case in the present study, which, instead of being able to show a clear causal connection, relies on circumstantial evidence and physical intuition. We combined the values of the eddy temperature advection with other information to understand the processes by which TIWs impact the ML heat budget. The smallness of the horizontal diffusion and the spatial structure of the TIW temperature advection (Fig. 4) or heat flux convergence (Fig. 5) shows that the mixing length paradigm cannot explain the equatorial warming due to TIWs. Stokes drift was also found to be small; therefore, it can be concluded that TIWs increase the atmosphere–ocean heat flux. TIWs move water toward patches of strong entrainment, be they due to equatorial Ekman divergence or equatorial wave dynamics. This cooling of the surface waters is balanced by a subsurface heating and causes a reduced latent heat loss of the ocean, which results in an increased net heat flux into the ocean.

It was shown previously in Jochum et al. (2005) that including this process into ocean models significantly changes the structure of near-equatorial SST. Therefore, it is important to validate the size of TIW temperature advection in the model with observations. To the best of our knowledge we resolved the horizontal structure of TIWs, but we shifted the problem from understanding TIW temperature advection to validating vertical entrainment and atmosphere–ocean heat fluxes, both of which are notoriously difficult to observe. One can argue, however, that, if the temperature advection in the model is similar to the observed values, the model represents TIWs, entrainment, and surface heat flux reasonably well.

Jayne and Marotzke (2002) showed that altimeter data, at least as it is currently used (see Stammer 1997), lead to large errors in estimating equatorial eddy temperature advection. Surface drifter data, too, are of doubtful utility for the present purpose. Because of its spatial and temporal distribution, it has to be averaged zonally to provide statistically meaningful results. One can then estimate the meridional gradient of the eddy temperature flux (Hansen and Paul 1984; Baturin and Niiler 1997). This method, however, assumes that zonal temperature advection is negligible. Otherwise ML warming will be spuriously assigned to meridional processes. Thus, if the present model has any fidelity,

drifter data as currently published cannot be used for validation.

To our knowledge there have been only two mooring-based field experiments with a spatial resolution sufficient to determine meridional temperature advection of TIWs: one in the Atlantic (Weisberg and Weingartner 1988) and one in the Pacific (Bryden and Brady 1989). Neither provides sufficient zonal resolution to determine the zonal temperature advection of TIWs, but Bryden and Brady found $(\overline{v'T'})_y$ to have a surface maximum at 0°, 110°W of $10 \pm 3 \times 10^{-7}$°C s^{-1} (their Fig. 8). Within the uncertainty, this is identical to the model value of $12 \pm 1 \times 10^{-7}$°C s^{-1}. This is reassuring, but considering the importance of TIWs for equatorial SST and tropical climate, the present results call for at least one high-density mooring experiment to determine not only the meridional but also the zonal temperature advection, which to our knowledge has never been measured.

The fact that the zonal component has never been measured is probably due to the dominance of the mixing length paradigm. Under this paradigm, there should be only limited zonal temperature advection, because of the weak zonal large-scale temperature gradient. Because of the absence of direct observations, the present authors looked at a range of available observations to see whether there is indirect evidence of zonal temperature advection. The available set of drifter data proved to be too small to arrive at a statistical meaningful estimate for the zonal temperature advection, but the observations by Kennan and Flament (2000) during the Tropical Instability Wave Experiment provide some support. A TIW was mapped over one wave period with ADCP sections, satellite infrared images, and 25 drifters. The mapping reveals that warm water indeed flows zonally across the SST front (their Fig. 14) and at 2°N produces a zonal temperature advection of approximately 0.5°C month^{-1}. This is about one-third of the annual mean in the model but it also representative of only one period.

Another valuable observation is provided by Johnson (1996). On crossing the SST front of the TIWs at 2°N he observes a drop in the Richardson number below the ML to 0.2, a strong indication for vertical entrainment. This is clearly north of the equatorial Ekman divergence and indicates that the mixing is due to TIWs.

Acknowledgments. The authors benefited from extensive discussions with R. Ferrari and the helpful suggestions of B. Fox-Kemper, J. Goodman, W. Large, and A. Plumb. This research was supported by NOAA funds for mesoscale air–sea interaction.

REFERENCES

Andrews, D., and M. McIntyre, 1976: Planetary waves in horizontal and vertical shear: The generalized Eliassen–Palm relation and the mean zonal acceleration. *J. Atmos. Sci.,* **33,** 2031–2048.

Baturin, N., and P. Niiler, 1997: Effects of instability waves in the mixed layer of the equatorial Pacific. *J. Geophys. Res.,* **102,** 27 771–27 793.

Boebel, O., C. Schmid, and W. Zenk, 1999: Kinematic elements of Antarctic Intermediate Water in the South Atlantic. *Deep-Sea Res.,* **46,** 355–392.

Boyd, J. P., 1976: The noninteraction of waves with the zonally averaged flow on a spherical earth and the interrelationships of eddy fluxes of energy, heat and momentum. *J. Atmos. Sci.,* **33,** 2285–2291.

Bryden, H., and E. Brady, 1989: Eddy momentum and heat fluxes and their effects on the circulation of the equatorial Pacific Ocean. *J. Mar. Res.,* **47,** 55–79.

Chavez, F., P. G. Strutton, C. E. Friederich, R. A. Feely, G. C. Feldman, D. C. Foley, and M. J. McPhaden, 1999: Biological and chemical response of the equatorial Pacific Ocean to the 1997–1998 El Niño. *Science,* **286,** 2126–2131.

Chelton, D. B., F. J. Wentz, C. L. Gentemann, R. A. de Szoeke, and M. G. Schlax, 2000: Satellite microwave SST observations of transequatorial tropical instability waves. *Geophys. Res. Lett.,* **27,** 1239–1242.

——, and Coauthors, 2001: Observations of coupling between surface wind stress and sea surface temperature in the eastern tropical Pacific. *J. Climate,* **14,** 1479–1498.

Chen, D., L. Rothstein, and A. Busalacchi, 1994: A hybrid vertical mixing scheme and its applications to tropical ocean models. *J. Phys. Oceanogr.,* **24,** 2156–2179.

Cox, M., 1980: Generation and propagation of 30-day waves in a numerical model of the Pacific. *J. Phys. Oceanogr.,* **10,** 1168–1186.

Cronin, M., 1996: Eddy–mean flow interaction in the Gulf Stream at 68°W. Part II: Eddy forcing on the time-mean flow. *J. Phys. Oceanogr.,* **26,** 2132–2151.

Dueing, W., and Coauthors, 1975: Meanders and long waves in the equatorial Atlantic. *Nature,* **257,** 280–284.

Eliassen, A., and E. Palm, 1961: On the transfer of energy in stationary mountain waves. *Geofys. Publ.,* **22,** 1–23.

Fox-Kemper, B., R. Ferrari, and J. Pedlosky, 2003: On the indeterminancy of rotational and divergent eddy fluxes. *J. Phys. Oceanogr.,* **33,** 478–483.

Gent, P., and M. Cane, 1989: A reduced gravity, primitive equation model of the upper equatorial ocean. *J. Comput. Phys.,* **81,** 444–480.

——, and J. McWilliams, 1990: Isopycnal mixing in ocean circulation models. *J. Phys. Oceanogr.,* **20,** 150–155.

Hansen, D., and C. Paul, 1984: Genesis and effects of long waves in the equatorial Pacific. *J. Geophys. Res.,* **89,** 10 431–10 440.

Hashizume, H., S. Xie, T. Liu, and K. Takeuchi, 2001: Local and remote atmospheric response due to tropical instability waves: A global view from space. *J. Geophys. Res.,* **106,** 10 173–10 185.

Hellerman, S., and M. Rosenstein, 1983: Normal monthly wind stress over the World Ocean with error estimates. *J. Phys. Oceanogr.,* **13,** 1093–1104.

Hoskins, B., I. N. James, and G. H. White, 1983: The shape, propagation and mean-flow interaction of large-scale weather systems. *J. Atmos. Sci.,* **40,** 1595–1612.

Jayne, S. R., and J. Marotzke, 2002: The oceanic eddy heat transport. *J. Phys. Oceanogr.,* **32,** 3328–3345.

Jochum, M., and P. Malanotte-Rizzoli, 2003: On the flow of Antarctic Intermediate Water along the equator. *Interhemispheric Water Exchanges in the Atlantic Ocean,* G. J. Goni and P. M. Malanotte-Rizzoli, Eds., Elsevier Oceanography Series, Vol. 68, Elsevier, 193–212.

——, and ——, 2004: A new driving mechanism for the South Equatorial Undercurrent. *J. Phys. Oceanogr.,* **34,** 755–771.

——, and R. Murtugudde, 2004: Internal variability in the tropical Pacific Ocean. *Geophys. Res. Lett.,* **31,** L14309, doi:10.1029/2004GL020488.

——, and P. Malanotte-Rizzoli, 2005: Reply. *J. Phys. Oceanogr.,* **35,** 1497–1500.

——, ——, and A. Busalacchi, 2004a: Tropical instability waves in the Atlantic Ocean. *Ocean Modell.,* **7,** 145–163.

——, R. Murtugudde, P. Malanotte-Rizzoli, and A. Busalacchi, 2004b: Internal variability in the Atlantic Ocean. *Ocean–Atmosphere Interaction and Climate Variability, Geophys. Monogr.,* Vol. 147, Amer. Geophys. Union, 181–187.

——, ——, R. Ferrari, and P. Malanotte-Rizzoli, 2005: The impact of horizontal resolution on the equatorial mixed layer heat budget in ocean general circulation models. *J. Climate,* **18,** 841–851.

Johnson, E. S., 1996: A convergent instability wave front in the central tropical Pacific. *Deep-Sea Res.,* **43B,** 753–778.

Katz, E., 1997: Waves along the equator in the Atlantic. *J. Phys. Oceanogr.,* **27,** 2536–2544.

Kennan, S. C., and P. J. Flament, 2000: Observations of a tropical instability vortex. *J. Phys. Oceanogr.,* **30,** 2277–2301.

Kessler, W. S., L. M. Rothstein, and D. Chen, 1998: The annual cycle of SST in the eastern tropical Pacific as diagnosed in an OGCM. *J. Climate,* **11,** 777–799.

Legeckis, R., 1977: Long waves in the eastern equatorial Pacific Ocean: A view from a geostationary satellite. *Science,* **197,** 1179–1181.

Levitus, S., 1994: *Climatological Atlas of the World Ocean.* NOAA Prof. Paper 13, 173 pp. and 17 microfiche.

Lindzen, R., 1988: Instability of plane parallel shear flow (toward a mechanistic picture of how it works). *Pure Appl. Geophys.*, **126,** 103–121.

Lyman, J. M., D. B. Chelton, R. A. deSzoeke, and R. M. Samelson, 2005: Tropical instability waves as a resonance between equatorial Rossby Waves. *J. Phys. Oceanogr.,* **35,** 232–254.

Marshall, J., and G. Shutts, 1981: A note on rotational and divergent eddy fluxes. *J. Phys. Oceanogr.,* **11,** 1677–1680.

Masina, S., and S. Philander, 1999: An analysis of tropical instability waves in a numerical model of the Pacific Ocean: 1. Spatial variability of the waves. *J. Geophys. Res.,* **104,** 29 613–29 635.

McCreary, J., 1981: A linear stratified ocean model of the equatorial undercurrent. *Philos. Trans. Roy. Soc. London,* **298,** 603–645.

——, and D. Anderson, 1984: A simple model of El Niño. *Mon. Wea. Rev.,* **112,** 934–946.

——, and P. Lu, 1994: Interaction between the subtropical and equatorial ocean circulations: The subtropical cell. *J. Phys. Oceanogr.,* **24,** 466–497.

McWilliams, J. C., and G. Danabasoglu, 2002: Eulerian and eddy-induced meridional overturning circulations in the Tropics. *J. Phys. Oceanogr.,* **32,** 2054–2071.

Menkes, C., and Coauthors, 2002: A whirling ecosystem in the equatorial Atlantic. *Geophys. Res. Lett.,* **29,** 1553, doi:10.102912001GL014576.

Murtugudde, R., R. Seager, and A. Busalacchi, 1996: Simulation of the tropical oceans with an ocean GCM coupled to an atmospheric mixed-layer model. *J. Climate,* **9,** 1796–1815.

Musman, S., 1986: Sea level changes associated with westward propagating equatorial temperature fluctuations. *J. Geophys. Res.,* **91,** 10 753–10 757.

——, 1992: *Geosat* altimeter observations of long waves in the equatorial Atlantic. *J. Geophys. Res.,* **97,** 3573–3579.

Pedlosky, J., 1987: An inertial theory for the equatorial undercurrent. *J. Phys. Oceanogr.,* **17,** 1978–1985.

——, 1996: *Ocean Circulation Theory.* Springer, 454 pp.

Philander, S., 1976: Instabilities of zonal equatorial currents. *J. Geophys. Res.,* **81,** 3725–3735.

——, 1978: Instabilities of zonal equatorial currents: 2. *J. Geophys. Res.,* **83,** 3679–3682.

——, 1990: *El Niño, La Nina and the Southern Oscillation.* Academic Press, 293 pp.

Plumb, R., 1983: A new look at the energy cycle. *J. Atmos. Sci.,* **40,** 1669–1688.

——, 1986: Three-dimensional propagation of transient quasi-geostrophic eddies and its relationship with the eddy forcing of the mean flow. *J. Atmos. Sci.,* **43,** 1657–1678.

Proehl, J., 1990: Equatorial wave-mean flow interaction: The long Rossby waves. *J. Phys. Oceanogr.,* **20,** 274–294.

——, 1996: Linear instability of equatorial zonal flows. *J. Phys. Oceanogr.,* **26,** 601–621.

Qiao, L., and R. Weisberg, 1995: Tropical instability wave kinematics: Observations from the Tropical Instability Wave Experiment. *J. Geophys. Res.,* **100,** 8677–8693.

——, and ——, 1998: Tropical instability wave energetics: Observations from the Tropical Instability Wave Experiment. *J. Phys. Oceanogr.,* **28,** 345–360.

Rudnick, D. L., H. W. Wijesekera, C. A. Paulson, and S. Pegau, 2002: Finescale upper ocean structure along 95W between 10N and 1S during EPIC. *Eos, Trans. Amer. Geophys. Union*, **83** (Suppl.), Abstract A22A-0068.

Schudlich, R., and J. F. Price, 1992: Diurnal cycles or current, temperature and turbulent dissipation in a model of the equatorial upper ocean. *J. Geophys. Res.,* **97,** 5409–5422.

Seager, R., M. Blumenthal, and Y. Kushnir, 1995: An advective atmospheric mixed layer model for ocean modeling purposes: Global simulation of atmospheric heat fluxes. *J. Climate,* **8,** 1951–1964.

Stammer, D., 1997: Global characteristics of ocean variability estimated from TOPEX/Poseidon altimeter measurements. *J. Phys. Oceanogr.,* **27,** 1743–1769.

Stevenson, J., and P. Niiler, 1983: Upper ocean heat budget during the Hawaii-to-Tahiti Shuttle Experiment. *J. Phys. Oceanogr.,* **13,** 1894–1907.

Weisberg, R., and T. Weingartner, 1988: Instability waves in the equatorial Atlantic Ocean. *J. Phys. Oceanogr.,* **18,** 1641–1657.

Yu, Z., J. McCreary, and J. Proehl, 1995: Meridional asymmetry and energetics of tropical instability waves. *J. Phys. Oceanogr.,* **25,** 2997–3007.